PUC

ISSN 0103-9741

Monografias em Ciência da Computação
n° 04/09

Automatic Embryonic Stem Cells Detection and Counting Method in Fluorescence Microscopy Images

Geisa Martins Faustino
Marcelo Gattass
Paulo Cezar Pinto Carvalho
Stevens Rehen
Carlos José Pereira de Lucena

Departamento de Informática

PONTIFÍCIA UNIVERSIDADE CATÓLICA DO RIO DE JANEIRO
RUA MARQUÊS DE SÃO VICENTE, 225 - CEP 22451-900
RIO DE JANEIRO - BRASIL

Monografias em Ciência da Computação, No. 04/09 ISSN: 0103-9741
Editor: Prof. Carlos José Pereira de Lucena February, 2009

Automatic Embryonic Stem Cells Detection and Counting in Fluorescence Microscopy Images

Geisa Martins Faustino, Marcelo Gattass, Paulo Cezar Pinto Carvalho, Stevens Rehen and Carlos José Pereira de Lucena

gfaustino@inf.puc-rio.br, mgattass@tecgraf.puc-rio.br, pcezar@impa.br, srehen@anato.ufrj.br, lucena@les.puc-rio.br

Abstract. In this paper, we propose an automatic embryonic stem cell detection and counting method in fluorescence microscopy images. We handle with pluripotent stem cells cultured *in vitro*. Our approach uses the luminance information to generate a graph-based image representation. Then, a graph mining process is used to detect the cells. The proposed method was extensively tested on a database of 92 images and the results were validated by specialists. We obtained an average precision, recall and F-measure of 93.97%, 92.04% and 92.87%, respectively.

Keywords: Automated cell counting, fluorescence microscopy images, graph based image representation, graph mining.

Resumo. Neste artigo, nós propomos um método automático para detecção e contagem de células tronco embrionárias em imagens de micrsocopia fluorescente. Nós lidamos com células tronco cultivadas *in vitro*. Nossa abordagem utiliza a informação de luminância para gerar uma representacão da imagem baseada em grafo. Então, um processo de mineração é utilizado para detectar as células. O método proposto foi exaustivamente testado numa base de dados composta por 92 imagens e os resultaos foram revisados por especialistas. Nós obtivemos uma *precision*, *recall* e *F-measure* média de 93.97%, 92.04% and 92.87%, respectivamente.

Palavras-chave: Contagem automática de células, imagens de micrsocopia fluorescente, representacão de imagem baseada em grafo, mineração de grafo.

In charge of publications:
Rosane Teles Lins Castilho
Assessoria de Biblioteca, Documentação e Informação
PUC-Rio Departamento de Informática
Rua Marquês de São Vicente, 225 - Gávea
22451-900 Rio de Janeiro RJ Brasil
Tel. +55 21 3527-1516 Fax: +55 21 3527-1530
E-mail: bib-di@inf.puc-rio.br
Web site: http://bib-di.inf.puc-rio.br/techreports/

1 Introduction

Embryonic stem cells are self-renewing elements that, through mitotic cell division and differentiation process, can generate all three germ layers (endoderm, ectoderm and mesoderm) and also specialized adult cells such as neurons, osteoblasts, cardiomyocytes, hepatocytes of the human body. They are found in various parts of the human body at every stage of development from embryo to adult and are classified according to their potential to develop into other cell types. A pleuripotent stem cell can develop into cells from all three germinal layers while multipotent stem cells can generate only closely related family of cells (e.g. hematopoietic stem cells differentiate into red blood cells, white blood cells, platelets, etc.). These characteristics of pluripotency make them a promising alternative for cell-based treatments of various diseases. Their differentiation process can be recapitulated by culturing those cells in non-adherent plates when cystic structures characterized by cavitations and fluid accumulation called embryoid bodies are formed.

Using different cell markers, specialists are able to determine, by manual counting, the total number of cells, how many specialized itself into a specific mature cell and how many cells died. These statistics are used to understand and validate the experiments. However, given the absence of high contrast, large number of cluttered objects in a single scene, occlusion, tuning in microscopy parameters and variability of cell size and morphology, detect and count these cells is a difficult task. Moreover, it requires a high level of concentration that makes manual screening a tedious and time-consuming task. In addition, the results are subjective and can greatly variate according to the personal interpretation of each specialist. Therefore, there is a strong motivation for the development of an automatic cell detection and counting method, which can be a useful tool for understanding and accelerating the stem cell therapy process.

There are methods [28, 21] to identify and quantify sections of cells cultured in suspension. However, these methods are expensive and require a trained technical specialist. Another disadvantage is that the spatial information is lost, because the cells must be separated. This information is important because the specialists are able to observe some phenomena, such as, the differentiated cells are located in the colony's extremity while the specialized stem cells are located at the colony's center [9].

Several researchers have been developing automated methods for segmenting and counting cells in microscopy images [29, 31, 5, 36, 11, 30, 4]. Some approaches are based on machine learning [22, 23, 34]. Long *et al.* [22] and Zheng *et al.* [34] proposed methods based on neural network and Markiewicz *et al.* [23] proposed a method to cell recognition and count using Support Vector Machine. In this kind of approach, the major task is to create the learning set, which is usually done manually by an independent expert for cell type. Another disadvantage is the time spend on training and parameter adjust. Approaches that use classical segmentation methods, such as threshold, morphological filtering and watershed transformation [3, 26, 12, 7] also have been proposed. With the discovery of the stem cells potential, many researches have been dealing with this kind of cell [24, 8, 18, 19, 2, 32, 15, 17, 16, 20]. Althoff *et al.* [2] and Tang *et al.* [32] proposed a method for segmentation and tracking of neural stem cells (NSC). Both approaches are based on classical segmentation methods and use the information about the cells' previous position to decide which blobs correspond to real cells. Also working with NSC, Korzynska [20] presented a method for automatic counting of neural stem cells growing in cultures which is performed in two steps: 1) segmentation step: the image is separated in several regions and; 2)counting step: each homogeneous region is counted separately. Some approaches handle with hematopoietic stem cells (HSC) [15, 17, 16]. Kachouie *et al.* [15] proposed a deconvolution method in the form of an optimized ellipse fitting algorithm to locate individuals HSC. The methods proposed in [17, 16],

uses the cell morphologic information (e. g. cell size, boundary brightness, interior brightness and boundary uniformity or symmetry) to locate and track HSC. Note that, the works cited above handled with only one type of stem cell in their images.

In this paper, we propose an automatic method for detecting and counting stem cells sections obtained under in fluorescence microscopy. We handle with embryoid bodies obtained from embryonic stem cells cultured *in vitro*. Our approach uses the luminance information to generate a graph-based image representation. Each cell is represented in the graph as a particular structure that we called *simple path*. Then, a graph mining process is used to detect the cells. While our motivation is to count stem cells, our approach can also be applied in other groups of objects, as long as the object surface are both smooth and concave with only one punctual illumination source. The proposed method was extensively tested on a database of 92 images and the results were validated by specialists. We obtained, in average, a precision, recall and F-measure of 93.97%, 92.04% and 92.87% respectively. We also have tested the proposed approach in others objects, such as seeds, candies and spots in electrophoresis images [13, 14]. Although counting cells are a well know problem, we are not aware of any other work that handles with several types of pluripotent stem cells in the same image.

The remainder of this paper is organized as follows: section 2 details the image characteristics; section 3 describes the proposed method; section 4 presents the experimental results to show the effectiveness of the method and; section 5 presents our conclusion and some future works.

2 Image Characterization

The images of embryoid bodies used in this work were collected in the Institute of Biomedical Sciences at UFRJ/Brazil. Shortly, embryoid bodies were cultured for 8 days under a neural differentiation process. In this procedure the embryoid bodies were stimulated to differentiate into a neural phenotype by the incubation, on the last 4 days, with retinoic acid at final concentration of $2\mu M$. After this time, they were fixed in 4% parafolmaldehyde (PF) solution for 30 minutes, passed through a sucrose gradient (10, 20 and 30%, 30 minutes each) and finally embeeded in tissue tek® OCT (optimum compound temperature) for cryopreserving. Slices were prepared on cryostat to discern the number of individual cells on each embryoid body. The slice thickness used was $10\mu m$, which corresponds to the nuclei average size. Next, the slices were incubated, for 5 minutes, with 4‘-6-Diamidino-2-phenylindole (DAPI), which is a kind of nuclei counter stain. The acquisition system consists of a Nikon Eclipse TE300 inverted epi-fluoresence microscope, a MagnaFire Digital CCD camera and the Image Pro Express software. The procedure of acquisition is semi-automatic and the specialist controls some parameters, such as, magnification, time exposure and focus. The resolution of the captured images were 1032×1040 pixels, which correspond to zoom of $40\times$. They were stored using Tagged Image File (.tif) format with lossless LZW compression. Figure 1 shows an example of a captured image.

Incorrect adjust of the microscopy parameters generate images with incorrect focus (Figure 2a). In these images, the edges become less clear and some cells are ignored by manual counting. Another difficulty is the partial occlusion of the cells. Although the slice thickness has the nuclei average size, some cells can be partially juxtaposed and they can appear partially occluded. This fact and the presence of many cells in a single scene (Figure 2b) are the main cause of slowness of the manual counting. Sometimes, it is very difficult to a human to distinguish the number of cells in a specific region. The DAPI binds to cell DNA and turning it visible, in blue/cyan, when visualized in the microscope. They appear lighter in the center and its luminance decreases

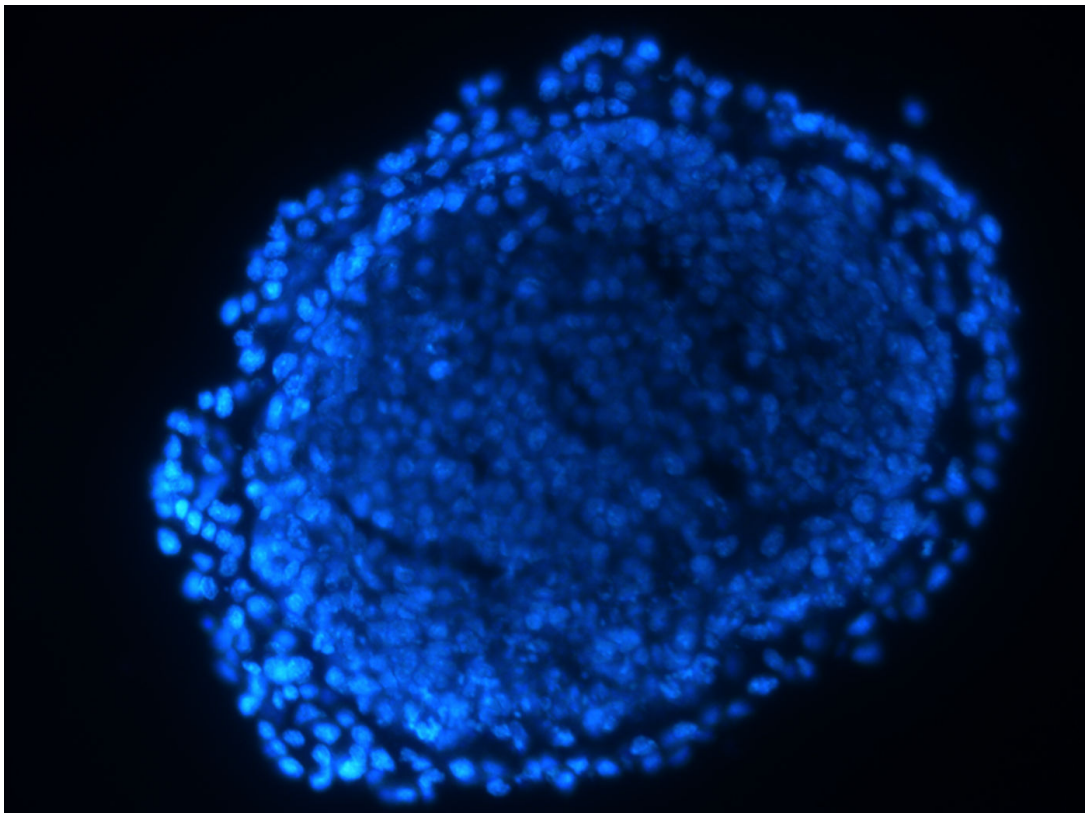

Figure 1: Captured stem cell image.

gradually. However, sometimes the DNA is more concentrated in different parts of the nuclei causing two or more lighter points in the same cell [27] (Figure 2c). When this occurs, the cell can be confused with two or more cells overlapped.

The occurrence of noise in captured images is natural (Figure 2d). However, the wrong choice of acquisition parameters produce different pattern of noise (Figure 2e) and stronger noise as in Figure 2f. The presence of noise and the other problems cited above make a challenge to develop an automatic counting method for embryonic stem cells. An advantage of such method is to avoid the subjectivity of the manual counting results, which is aggravated by these issues. In the next section we present a new method for detecting and counting embryoid bodies formed by embryonic stem cells undergoing differentiation in the images characterized in this section.

3 Proposed Method

In this section, we describe the proposed procedure to detect and count embryonic stem cells in microscopy fluorescence images automatically. These images, as the ones presented in section 2, have an interesting characteristic: the pixels of a cell are lighter in the middle and the pixel luminance value decreases gradually as it reaches the cell boundaries. We explore the luminance information by considering the image as a topological surface, where each pixel is a point situated at some altitude as a function of its grey level. Most precisely: let $I : \Omega \in \mathbb{Z}^2 \longrightarrow \mathbb{Z}$ be a function of gray levels representing a digital image. We have that, the graphic of I is a topological surface

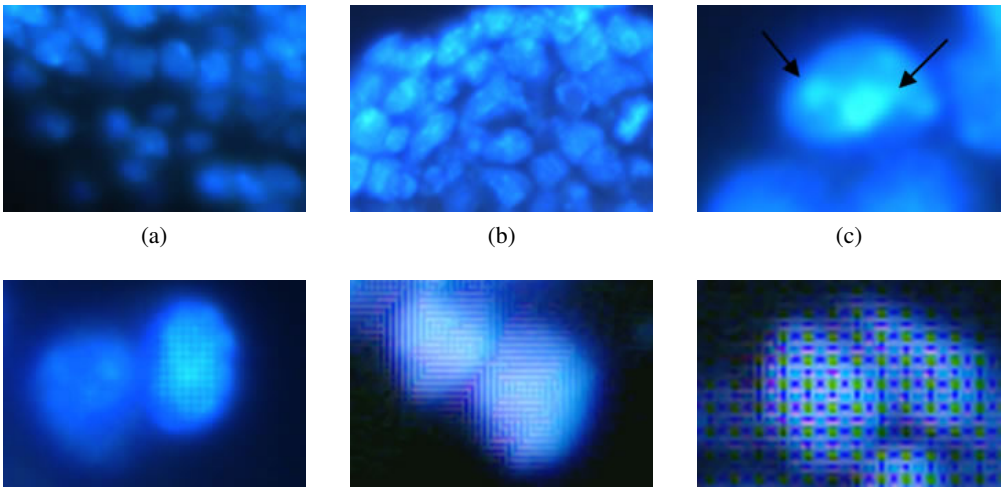

(a) (b) (c)

(d) (e) (f)

Figure 2: Image features: a) image out of focus; b) partial occlusion and many objects in a single scene; c) the DNA condensation phenomena [27] (the black arrows point out the two lighter points); d) presence of acceptable level of noise; e) presence of weak noise and; f)presence of strong noise.

in which the altitude of every point is equal to the gray level of the corresponding pixel (see Figure 3). Moreover, we have that each cell can be identified as a set of local maximum points, because the presence of noise and the DNA condensation phenomena. Therefore, the classical methods [25, 6] cannot be applied directly. The method proposed in [6] generate an over segmentation and many artifacts are classified, wrongly, as cell. The method proposed in [25], uses a neighborhood of fix size and all pixels whose intensity is not maximal within this neighborhood are ignored. Thus, if there are more than one cell in this region, only one are counted. On the other hand, if the region size is too small many artifacts are classified, wrongly, as cell.

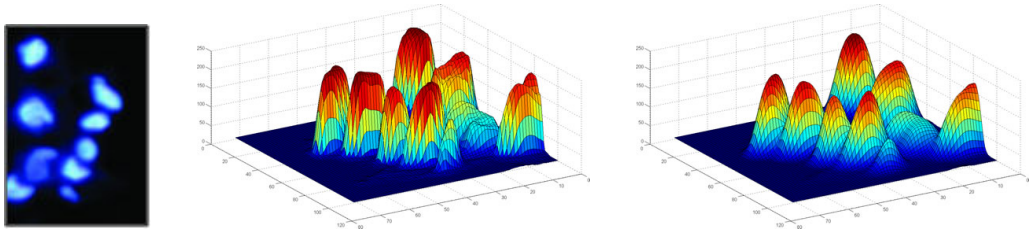

(a) (b) (c)

Figure 3: Surface plot: a) input image; b) surface plot and c) surface plot after a Gaussian blur filter. Note that in b), due to presence of noise and the DNA condensation phenomena, one cell is represented by a set of maximum point. However, after the Gaussian filter, because it smoothed the surface and emphasize the maximum points, many cells are represented by only one local maximum point.

We detected local maximum points tracing level curves in which the set of points $(x, y) \in \Omega$ that satisfies $c \leq I(x, y) < c + \varepsilon$, where $c, \varepsilon \in \mathbb{Z}_+$, corresponds to the image pixels that belongs

to the level c. Likewise, this can be done parting the histogram image as described below. For this images, the green channel supply more information than the gray scale image. Thus, our luminance information is based on this channel.

Our method has four main steps: 1) pre-processing; 2) histogram partition and connected component detection; 3) graph construction; and 4) graph mining process, which we shall discuss in the sequel.

3.1 Preprocessing

A Gaussian filter, with radius σ, is applied to reduce the noise and emphasize the maximum points as showing in Figure 3. Furthermore, as the background image is not uniform, due to fluorescence, a background segmentation is applied. We separate the cells agglomerate from background using a threshold $t = \mu + x\delta$, where μ is the mean value of image, σ is the image standard deviation and x is a constant defined experimentally. The pixels with intensity below t are set to 0. Figure 4 presents the results of each step. In Figure 4a and b we have the input image and its green channel, respectively. The result after Gaussian blur filter is showed in Figure 4c. Finally, Figure 4d presents the result of background segmentation.

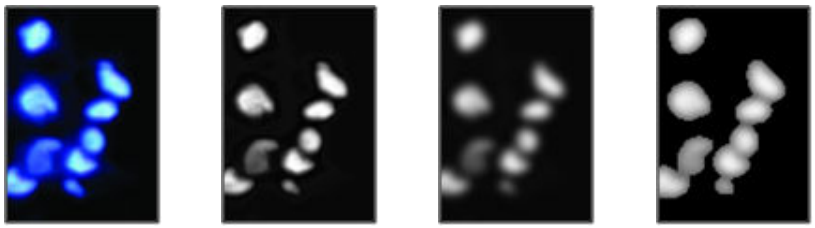

(a) (b) (c) (d)

Figure 4: Pre-processing steps: a) input image; b) green channel; c) result of Gaussian blur filter; d) result of background segmentation.

3.2 Histogram Partition and Connected Component Detection

The goal of this step is detect the connected components in each bitmap created by histogram partition. We start calculating the histogram of I. The second step, is partition the histogram in intervals of size ε and identify what pixels belong to each interval. In this work, ε is a divisor of 256. As we are deal with discrete value, the size of an interval $[a, b]$ is $(b - a) + 1$. Thus, given an interval $[a, b]$ such as $(b - a) + 1 = \varepsilon$ and a pixel $p \in \Omega$, we have that $p \in [a, b] \Leftrightarrow a \leq I(p) \leq b$. For each interval, we construct a bitmap, such that, the black pixels correspond to the pixels belonging to the current interval. Figure 5a shows the histogram of Figure 4e and the bitmaps for each interval. In this example, we use $\varepsilon = 64$. Therefore, we have a partition composed by four intervals. Note that, the nine cells existing in the input image (Figure 4a) appear in the first two bitmaps.

The next step is to find the 8×8 connected components of the bitmaps according to the algorithm described in [10]. We start from the bitmap that corresponds to the interval $[255 - (\varepsilon - 1), 255]$ and continue until the interval $[0, \varepsilon - 1]$. Each component receives a label (just an integer number) according to the order which it was detected. Thus, we guaranty an order of the component label value, such that, higher its value smaller is the luminance of the component.

As a result of this step, we have a matrix $M_{m \times n}$ with same dimensions of input image, where each entry $M(i, j)$ contains the component label value that the pixel $p(i, j)$ belongs to. Most precisely:

$$M(i, j) = k \Leftrightarrow p(i, j) \in C_k \text{ for some } 1 \leq k \leq R$$

where $p(i, j) \in \Omega$ is a pixel image and R is the total number of connected components that were detected.

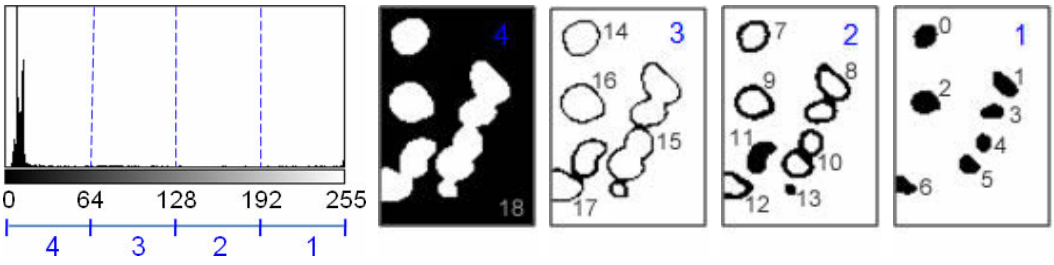

(a) (b) (c) (d) (e)

Figure 5: Histogram partition and connected components detection: a) histogram of Figure 4e; b), c) d) and e) bitmaps representing the intervals 4) $[0, 63]$, 3) $[64, 127]$, 2) $[128, 191]$, and 1) $[192, 255]$, respectively. The gray numbers are the label of the connected component. Note that the higher is the label value smaller is the luminance of the component.

3.3 Graph Construction

The goal of this step is construct a region-adjacency graph (RAG) [33] $G = (V, E)$ based on the matrix M. Each node $v_i \in V$ correspond to a connected component and its index corresponds to the component label value. The edges in E connects pairs of 4×4 adjacent components in accordance with the definition 3.1.

Definition 3.1 *Two distinct components C_i and C_j are said to be adjacent if there is at least a pair of points $p_i \in C_i$ and $p_j \in C_j$, which are neighbors of each other.*

Thus, in order to construct the graph, we scan M from top to bottom and left to right evaluating the top and left neighbors of each element of M. If one of them are different from the current element, then these elements represent pixels that belong to different connected components. Thus, according to definition 3.1 these components are adjacent and therefore, have to be an edge in the graph connecting the nodes that represent them. Figure 6a shows all connected components that were detected on Figure 4a and their labels. The adjacency graph correspondent is presented in Figure 6b. Note that the nodes with smaller indexes are located at the graph extremity.

3.4 Graph Mining

We are interested in detecting regions of image that have the following pattern: a lighter region whose luminance adjacency regions are being decreased gradually. Note that, if a set of connected components belongs to the same object, then they have to be adjacent. Therefore, the nodes which represent them in G, have to be connected. Note also that, the node index has the same value of the component label and higher its value smaller is the luminance of the component. Thus, we have that the pattern above can be identified in G by *simple paths* (see Definition 3.2).

Definition 3.2 *A **simple path** in a graph $G = (V, E)$ can be defined as a subgraph S that satisfy:*

i) the nodes in S are connected to other nodes in S;

ii) each node of S has a maximum degree of two and;

iii) the index value of a node is smaller than the one of its adjacent node and bigger than the one of other adjacent node, if it exists (i.e. the index values of the nodes in S are in increasing order).

Figure 6b shows the input image graph-based representation. Note that since all nodes are adjacent, at least, to the background, there are not nodes with degree 0. Figure 6c presents the result of the mining process, that is, the detected simples paths. We have that each cell presented in input image (Figure 4a) is represented in G by a simple path, even it has only one node. Another interesting characteristic is that if a node has degree bigger than 2, the component that it represents contains more than one cell and therefore can not be classified neither as a new cell nor as belonging to some cell (see Figure 6a, components 15, 17 and 18, for example).

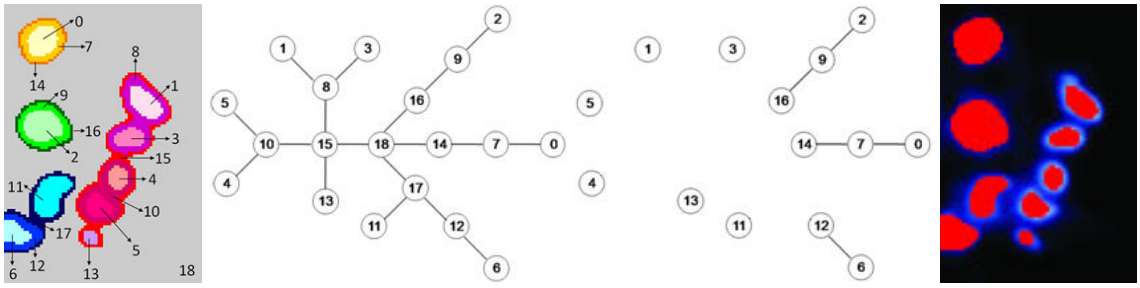

(a) (b) (c) (d)

Figure 6: Graph representation and mining step: a) connected components detected and their labels; b) input image graph-based representation; c) result of the graph mining process; and d) cells detected in red.

The graph mining process allows us detect and count cells by discovering simple paths. The input is a graph $G = (V, E)$, with n nodes and m edges and the output is the set $A = \alpha_1, \alpha_2, \ldots, \alpha_k$ where each $\alpha_i = \{v_i, v_j, v_k, \ldots, v_l | i < j < k < \cdots < l\} \in A$ is a simple path representing a detected cell. All nodes in G are initialized as belonging to any cell and as not visited. Starting from the node v_0, we iterate in V, in increasing order evaluating the nodes that have degree less than 3. These nodes, are classified according to their neighbor as a new cell or belonging to a some cell that was detected previously. Let v_i be the node that has been evaluated. If v_i is classified as a new cell, then an element α_i is created, v_i is associated to it and α_i added in A. On the other hand, if v_i belongs to a some cell, e.g. k^{th} cell, it is associated to element $\alpha_k \in A$. At the end, the node v_i is set as visited. The nodes are classified as described as follows:

The degree of the node v_i is 1 It is classified as a new cell if: its neighbor, v_j, was not visited yet or v_j was visited but classified as belonging to any cell. On the other hand, if v_j was already visited and belongs to some cell, e.g. k^{th} cell, we have that v_i also belongs to this cell.

The degree of the node v_i is 2 Let v_j and v_k be its neighbors. We have six possibilities: 1) v_j and v_k was already visited and both was classified as belonging to the same cell, e.g. m^{th} cell; 2) v_j and v_k was visited and classified as belonging to any cell; 3) v_j and v_k was visited and classified as belonging to different cells; 4) one of them, e.g. v_j, was visited and classified as belonging to some cell e.g. m^{th} cell, and the other, v_k, was not visited yet; 5) one of them, e.g. v_j, was visited and classified as belonging to some cell e.g. m^{th} cell, and the other, v_k was visited and classified as belongs to any cell; and 6) v_j and v_k was not visited yet. If 1), 4) or 5) occur, v_i is classified as belonging to the m^{th} cell. If 2) or 3) occur, we can not associate v_i to any element of A because we find out a component that contains more than one cell. If 6) occur, as we are going through V in increasing order, we find a new cell.

4 Experimental Results

In this section, we evaluate the proposed method and analyze the experimental results. The proposed method was implemented in Java language 6.0 using the development tool Eclipse 3.2. The tests were executed on an Intel Core 2 Duo CPU T7500 2.20GHz with 2Gb RAM.

A database with 92 images of stem cells was constructed and divided in two groups: group 1, with 69 images with an acceptable level of noise and; group 2 formed by 23 images with the presence of strong noise. Additional experiments were performed for a third image group composed by 5 images of seeds, candies and spots in electrophoresis images [13]. The values for the input parameters σ, x and ε of the preprocessing step were obtained through experimental tests. The value for the Gaussian radius σ were 2,3 and 3 for the groups 1, 2 and 3, respectively. The threshold t were calculated using $x = 0.3$ for all groups. The histogram were partitioned in intervals of size $\varepsilon = 8$ for the groups 1 and 2. For the third group, the value of ε was chosen among 8, 16 and 32 that best fitted each image.

Specialists from Institute of Biomedical Sciences – UFRJ/Brazil validated the experimental results obtained by the proposed method. They pointed out cells that were not counted and artifacts that were incorrectly classified as cells. The results are evaluated by calculating the measures precision, recall and F-measure as shown as follow:

$$Precision = \frac{tp}{tp + fp} \tag{1}$$

$$Recall = \frac{tp}{tp + fn} \tag{2}$$

$$F - measure = \frac{2 * Precision * Recall}{Precision + Recall} \tag{3}$$

where tp (true positives) represents the number of items correctly labeled as a cell, fp (false positives) represents items incorrectly classified, by the method, as a cell and fn (false negatives) represents items that were not classified as cell but should have been. The measures were calculated for each image and, then, averaged over all images. The results are presented in Table 1.

Note that the precision increased on the second group, while the recall and F-measure decreased. Since an aggressive Gaussian blur was required, the image contrast reduced and, as a result, fewer cells were detected increasing the number of false negative elements. On the other hand, fewer artifacts were incorrectly classified as cell that decreases the number of false positives.

	Precision (%)	**Recall** (%)	**F-measure** (%)
Group 1	93.84	92.67	93.12
Group 2	94.32	90.33	92.18
Group 1 and 2	93.97	92.04	92.87
Group 3	94.08	98.15	95.96

Table 1: Experimental results of the proposed method. All numbers are averaged values over all images.

Tables 2 and 3, at Appendix 6, presents the results for all images of groups 1 and 2, respectively. For the 92 images, we obtained an average precision, recall and F-measure of 93.97%, 92.04% and 92.87%, respectively. These numbers indicate the concordance with the human experts results. In addition, this is sufficiently accurate for biological practices. In manual counting, performed by the specialists, the difference of counting scores were 21% in average and a surprisingly maximum of 59%. Figure 7 shows the subjectivity of manual counting results for five experts. In this example, there was a mean perceptual error of 39% among their scores results. Furthermore, we observed that if the interval size ε is large, we cannot detect cells that have luminance value similar and that are partially overlapped. These cells are counted as only one cell. On the other hand, if the value of ε is too small, we detect many artifacts that are not cells.

Because of the image quality, which depends on a microscope type, resolution of acquired image and focus [1, 35], in some image regions, only with visual inspection, is very difficult to detect the cells. As a consequence, these regions are ignored by specialists. Nevertheless, according to them and by experimental results, the proposed method was able to detect cells in regions that they could not. Figures 8 and 9 shows examples of manual and automatic counting for six images. Note that the automatic counting method detects some cells that were ignored by manual counting.

The average time spent on each image by a human expert is 15 minutes. The proposed method performs it in 6.2 seconds, in average. Moreover, the counting results of the same human expert, on the same image, may vary up to 10%, while the algorithm, obviously, gives always the same result. Another advantage is that, with the automatic counting, we can eliminate the subjectivity because, unlike in manual counting, is guaranteed that the same criteria are always used to detect cells.

For additional experiments, we obtained an average precision, recall and F-measure of 94.08%, 98.15%, and 95.96%, respectively as showing in Table 1. Table 4, in Appendix A, shows the scoring results, measures and the value of input parameter ε for the images present in Figure 10 a, b, c and f. We noted that, for images where the partial occlusion of the objects is less intense, large values of ε gives better results. On the other hand, if several objects are overlapped, then better results are achieved using a small value for ε. The test images and the correspondent counting results are available at `http://www.inf.puc-rio.br/~gfaustino/cellcounter/`.

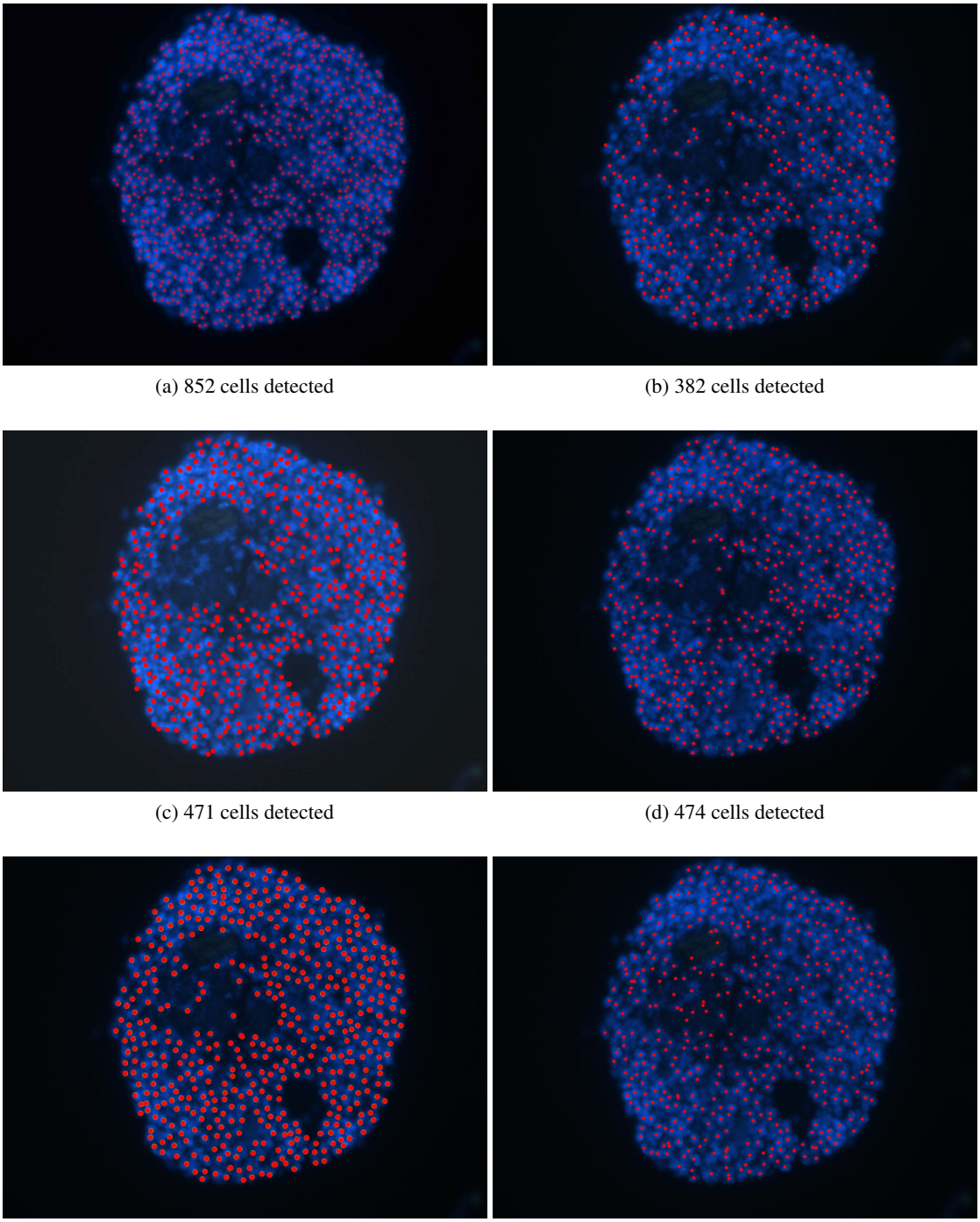

(a) 852 cells detected

(b) 382 cells detected

(c) 471 cells detected

(d) 474 cells detected

(e) 499 cells detected

(f) 435 cells detected

Figure 7: Subjectivity of manual count result by five different specialists: in this case, there was a mean perceptual error of 39.7%. f) shows the automatic counting result for the same image.

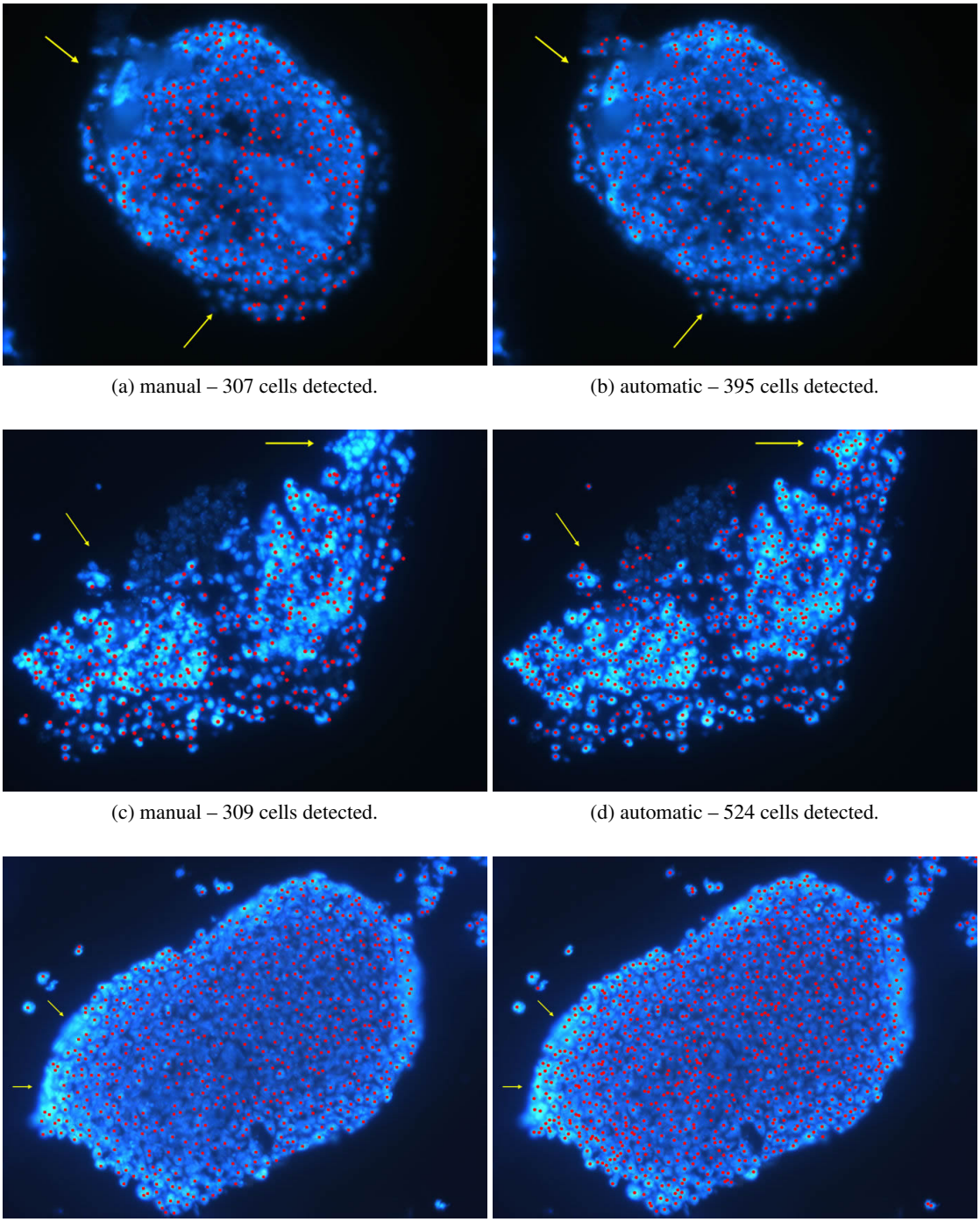

(a) manual – 307 cells detected.

(b) automatic – 395 cells detected.

(c) manual – 309 cells detected.

(d) automatic – 524 cells detected.

(e) manual – 636 cells detected.

(f) automatic – 916 cells detected.

Figure 8: Results of the manual and automatic counting: the red dots represent the cells that were detected and the yellow arrows point out the image regions ignored by the specialist but not by the automatic counting. The results of the proposed method were revised by specialist and we obtained F-measure of 89%, 92% and 96% for images b, d and f, respectively.

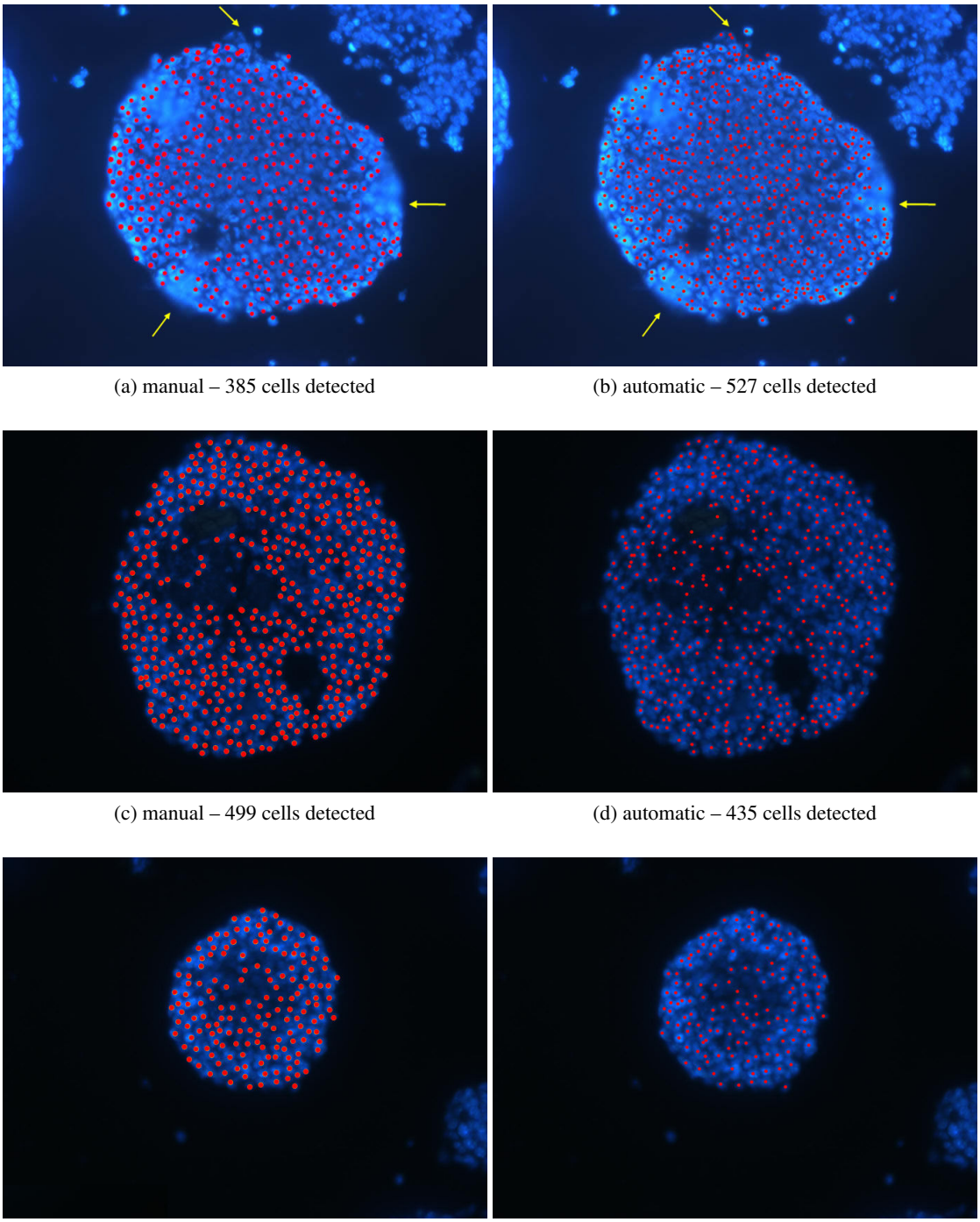

(a) manual – 385 cells detected

(b) automatic – 527 cells detected

(c) manual – 499 cells detected

(d) automatic – 435 cells detected

(e) manual – 163 cells detected

(f) automatic – 143 cells detected

Figure 9: Results of the manual and automatic counting: the red dots represent the cells that were detected and the yellow arrows point out the image regions ignored by the specialist but not by the automatic counting. Note that, in the last two images, the automatic method detected fewer cells than specialist. It occurs because the image contrast is smaller than usual. Then, many cells have the luminance value very similar and ones that are partially overlapped are counted as only one cell. The automatic count results were revised by specialist and for these images we obtained an F-measure of 92%, 86% and 88% for images b, d and f, respectively.

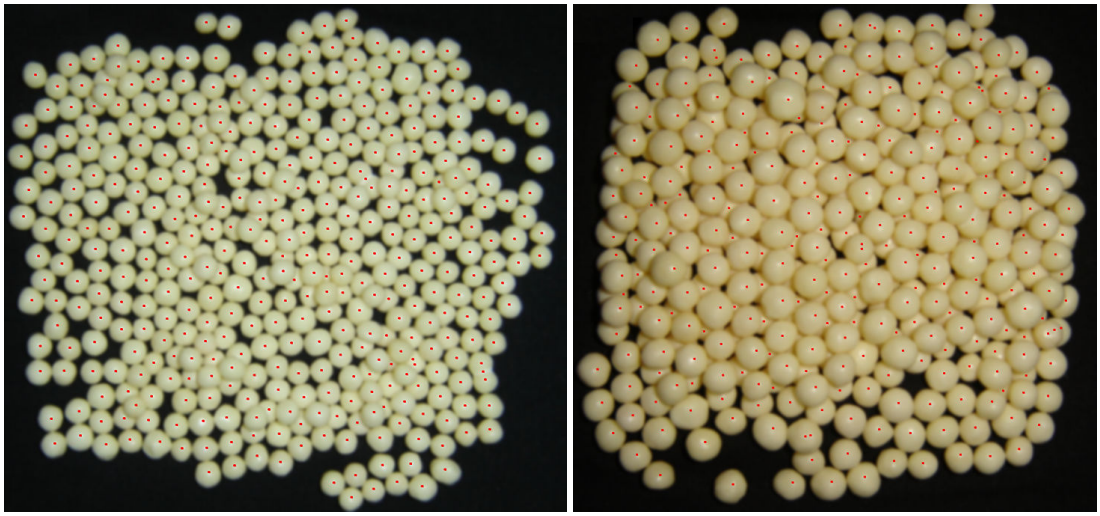

(a) objects detected – 393; manual count – 396

(b) objects detected – 321 ; manual count – 355

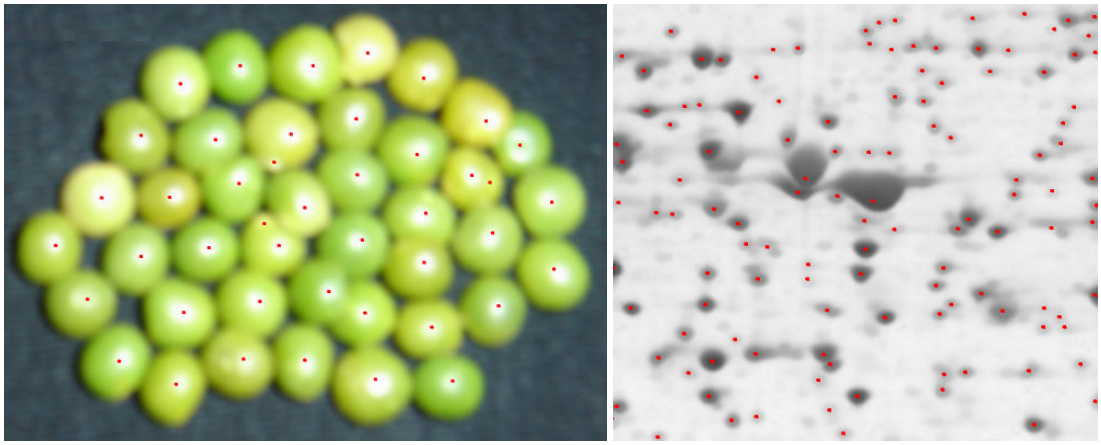

(c) objects detected – 44; manual count – 41

(d) objects detected – 122; manual count – 182

(e) objects detected – 40; manual count – 46

Figure 10: Additional examples of counting results by the proposed method, the red dots represent the objects that were detected: a) and b) candies; c) peas; d) two-dimensional gel electrophoresis images and e) withe beans.

5 Conclusion and Future Works

In this work, an automatic method for detecting and counting stem cells sections obtained under fluorescence microscopy was presented. We handle with embryoid bodies obtained from embryonic stem cells cultured *in vitro*. Our approach uses the luminance information to generate a graph-based image representation. Each cell was represented by a substructure that we called simple path pattern. Then, a graph mining process is used to detect such pattern. The accuracy of the proposed method was demonstrated with experimental results in a large population of stem cells image. The results was validated by specialists from Institute of Biomedical Sciences – UFRJ/Brazil. We obtained an average precision, recall and F-measure of 93.97%, 92.04% and 92.87%, respectively, which is satisfactory. Moreover, with the automatic counting, we can eliminate the subjectivity because, unlike in manual counting, is guaranteed that the same criteria are always used to detect cells. In addition, the results obtained in another kinds of images demonstrate that the method could be used in others applications.

Most counting errors performed by the proposed method are due to the existence of more than one lighter points at the same cell. Future work involves solving such problem by implementing a node contraction algorithm using their Euclidean distance as a criteria.

Acknowledgments

Thanks are due to Bruno Ávila and Aristófanes C. Silva for their most valuable assistance and to the team of collaborators, specially Priscila Brito - student of Institute of Biomedical Sciences – UFRJ/Brazil. The team helped us in the algorithm validation, with some discussions around the research hypothesis. The authors are supported by CAPES.

References

[1] B. Alberts, D. Bray, J. Lewis, M. Raff M, K. Roberts, and J. D. Watson. Molecular biology of the cell. *Garland Publishing Inc.*, (3), 1994.

[2] K. Althoff, J. Degerman, and T Gustavsson. Combined segmentation and tracking of neural stem-cells. In *Image Analysis*, pages 282 – 291. 2005.

[3] F. Ambriz-Colín, M. Torres-Cisneros, J. G. Avina-Cervantes, J. E. Saavedra-Martinez, O. Debeir, and J. J. Sanchez-Mondragon. Detection of biological cells in phase-contrast microscopy images. In *MICAI*, pages 68 – 77, 2006.

[4] Dwi Anoraganingrum. Cell segmentation with median filter and mathematical morphology operation. In *ICIAP*, 1999.

[5] P. Bamford. *Segmentation of cell images with an application to cervical cancer screening*. PhD thesis, University of Queenland, 1999.

[6] A. Bieniek and A. Moga. An efficient watershed algorithm based on connected components. 33(6):907–916, 2000.

[7] J. Degerman, J. Faijerson, K. Althoff, T. Thorlin, and T. Gustavsson. A comparative study between level set and watershed segmentations for tracking stem cells in time-lapse microscopy. In *Workshop on Microscopic Image Analysis with Applications in Biology*, pages 60 – 64, 2006.

[8] Takahashi et al. Induction of pluripotent stem cells from adult human fibroblasts by defined factors. *Cell*, 5(131):861 – 72, 2007.

[9] Lucena C. J. P. Faustino G., Gatti M. and Gattass M. A 3d multi-scale agent-based stem cell self-organization. *SEAS*, pages 37 – 48, 2008.

[10] Mark A. Foltz. Connected components in binary images. 6.866: Machine Vision, December 1997.

[11] A. Garrido and N. PeHrez de la Blanca. Applying deformable templates for cell image segmentation. *Pattern Recognition*, 33(5):821 – 832, 2000.

[12] E. Glory, A. Faure, V. Meas-Yedid, F. Cloppet, Ch Pinset, G. Stamon, and J-Ch Olivo-Marin. A quantification tool to analyse stained cell cultures. In *Image Analysis and Recognition*, pages 84 – 91. 2004.

[13] Minh-Tuan Trong Hoang and Yonggwan Won. A marker-free watershed approach for 2d-ge protein spot segmentation. *ISITC*, pages 161 – 165, 2007.

[14] K. D. Iakovidis, E. Zacharia, and S. Kossida. A genetic approach to spot detection in two-dimensional gel electrophoresis images. *ITAB*, 2006.

[15] N. N. Kachouie, P. Fieguth, and E. Jervis. Stem-cell localization: A deconvolution problem. In *EMBS*, pages 5525 – 5528, 2007.

[16] N. N. Kachouie, Paul Fieguth, John Ramunas, and Eric Jervis. Probabilisticmodel-based cell tracking. *Int. Journal of Biomedical Imaging*, pages 1 – 10, 2006.

[17] N. N. Kachouie, L. J. Lee, and P. Fieguth. A probabilistic living cell segmentation model. In *ICIP*, pages 137 – 140, 2005.

[18] N.N. Kachouie and P.W. Fieguth. A narrow-band level-set method with dynamic velocity for neural stem cell cluster segmentation. In *ICIAR*, pages 1006–1013, 2005.

[19] N.N. Kachouie, P.W. Fieguth, J. Ramunas, and E. Jervis. A model-based hematopoietic stem cell tracker. In *ICIAR*, pages 861–868, 2005.

[20] Anna Korzynska. Automatic counting of neural stem cells growing in cultures. In *Computer Recognition Systems*, pages 604 – 612. 2007.

[21] Julie Logan, Kirstin Edwards, and Nick Saunders. *Real-Time PCR: Current Technology and Applications*. Caister Academic Press, 2009.

[22] Xi Long, W. Louis Cleveland, and Y. Lawrence Yao. Effective automatic recognition of cultured cells in bright field images using fisher's linear discriminant preprocessing. *Image and Vision Computing*, 23(13):1203 – 1213, 2005.

[23] T. Markiewicz, S. Osowski, J. Patera, and W. Kozlowski. Image processing for accurate cell recognition and count on histologic slides. *Int. Academy of Cytology and American Society of Cytology*, 28(5):281 – 291, 2006.

[24] Inkyu Moon and Bahram Javidi. Three-dimensional identification of stem cells by computational holographic imaging. *J. R. Soc. Interface*, 4:305 – 313, 2006.

[25] Alexander Neubeck and Luc Van Gool. Efficient non-maximum suppression. In *ICPR*, volume 3, pages 850–855, 2006.

[26] Antti Niemisto, Limei Hu, Olli Yli-Harja, Wei Zhang, and Ilya Shmulevich. Quantification of in vitro cell invasion through image analysis. *EMBS*, pages 1 – 5, 2004.

[27] M. D. Stewart Sell. *Stem Cells Handbook*. Humana Press, 2003.

[28] S. Sergent-Tanguy, C. Chagneau, I. Neveu, and Naveilhan P . Fluorescent activated cell sorting (facs): a rapid and reliable method to estimate the number of neurons in a mixed population. *Journal of Neuroscience Methods*, 129(1):73 – 79, 2003.

[29] H. Sheikh, Bin Zhu, and E. Micheli-Tzanakou. Blood cell identification using neural networks. In *IEEE Twenty-Second Annual Northeast Bioengineering Conference*, pages 119–120, 1996.

[30] S. Shiotani, T. Fukuda, F. Arai, N. Takeuchi, K. Sasaki, and T. Kinoshita. Cell recognition by image processing: (recognition of dead or living plant cells by neural network). *JSME*, 37:202 – 208, 1994.

[31] Timthy Spencer, John A. Olson, Kenneth C. Mchardy, Peter R. Sharp, and John V. Forrester. An image-processing strategy for the segmentation and quantification of microaneurysms in fluorescein angiograms of the ocular fundus. *Computers and Biomedical Researches*, 29:284 – 302, 1996.

[32] C. Tang and E. Bengtsson. Segmentation and tracking of neural stem cell. In *Advances in Intelligent Computing*, pages 851–859. 2005.

[33] A. TREMEAU and P. COLANTONI. Regions adjacency graph applied to color image segmentation. *EEE transactions on image processing*, 9(4):735 – 744, 2000.

[34] Q. Zheng, B. K. Milthorpe, and A. S. Jones. Direct neural network application for automated cell recognition. *Cytometry A*, 57(1):1–9, 2004.

[35] D. Zicha and G. Dann. Molecular biology of the cell. *Journal of Microscopy*, 3:11 – 21, 1995.

[36] C. Zimmer, E. Labruyère, V. Meas-Yedid, N. Guillén, and JC. Olivo-Marin. Improving active contours for segmentation and tracking of motile cells in videomicroscopy. *16th Int. Conference on Patter Recognition*, 2:286 – 289, 2002.

6 Appendix A

In this appendix, we show the measures for all images used in the experimental results. In the first column we have the image file name, in the second column the number of cells detected with automatic counting. The three next column show the number of false positive (fp) representing items incorrectly classified as a cell, false negative (fn) representing items which were not classified as cell but should have been and true positive (tp) representing items correctly labeled as a cell, respectively. All these elements were point out by the specialists from Institute of Biomedical Sciences – UFRJ/Brazil that revised the results. Precision can be seen as a measure of exactness or fidelity, whereas Recall is a measure of completeness. F1-measure, is a measure of a test's accuracy and can be interpreted as a weighted average of the precision and recall. They reach their best value at 1 and worst score at 0.

Image	Automatic Counting	FP	FN	TP	Precision	Recall	F-measure
1	509	30	29	479	0.941060904	0.942913386	0.941986234
2	284	21	23	263	0.926056338	0.91958042	0.922807018
3	564	19	47	545	0.966312057	0.920608108	0.942906574
4	388	13	51	375	0.966494845	0.88028169	0.921375921
5	330	21	24	309	0.936363636	0.927927928	0.932126697
6	318	10	21	308	0.968553459	0.936170213	0.952086553
7	420	9	41	411	0.978571429	0.909292035	0.94266055
8	519	17	25	502	0.967244701	0.95256167	0.959847036
9	645	22	37	623	0.965891473	0.943939394	0.954789272
10	400	11	36	389	0.9725	0.915294118	0.943030303
11	406	20	33	386	0.950738916	0.92124105	0.935757576
12	559	36	32	523	0.935599284	0.942342342	0.938958707
13	212	16	12	196	0.924528302	0.942307692	0.933333333
14	352	19	23	333	0.946022727	0.935393258	0.940677966
15	642	22	62	620	0.965732087	0.909090909	0.936555891
16	403	9	15	394	0.977667494	0.963325183	0.97044335
17	419	30	30	389	0.928400955	0.928400955	0.928400955
18	276	16	21	260	0.942028986	0.925266904	0.933572711
19	522	60	26	462	0.885057471	0.946721311	0.914851485
20	717	34	90	683	0.952580195	0.883570505	0.916778523
21	278	34	6	244	0.877697842	0.976	0.924242424
22	458	23	54	435	0.949781659	0.889570552	0.918690602
23	598	73	14	525	0.877926421	0.974025974	0.92348285
24	464	52	17	412	0.887931034	0.96037296	0.922732363
25	368	16	58	352	0.956521739	0.858536585	0.904884319
26	425	27	38	398	0.936470588	0.912844037	0.924506388
27	499	23	30	476	0.953907816	0.940711462	0.947263682
28	401	58	14	343	0.855361596	0.960784314	0.905013193
29	522	54	22	468	0.896551724	0.955102041	0.924901186
30	629	32	45	597	0.949125596	0.929906542	0.939417781
31	448	17	33	431	0.962053571	0.92887931	0.945175439
32	262	29	4	233	0.889312977	0.983122363	0.933867735

Image	Automatic Counting	FP	FN	TP	Precision	Recall	F-measure
33	185	11	26	174	0.940540541	0.87	0.903896104
34	760	92	24	668	0.878947368	0.965317919	0.920110193
35	592	29	54	563	0.951013514	0.912479741	0.931348222
36	537	42	28	495	0.921787709	0.946462715	0.933962264
37	359	18	30	341	0.949860724	0.919137466	0.934246575
38	441	22	33	419	0.950113379	0.92699115	0.938409854
39	790	60	68	730	0.924050633	0.914786967	0.919395466
40	561	25	55	536	0.95543672	0.906937394	0.930555556
41	474	28	21	446	0.94092827	0.95503212	0.947927736
42	615	35	22	580	0.943089431	0.96345515	0.953163517
43	761	31	32	730	0.959264126	0.958005249	0.958634274
44	589	52	14	537	0.911714771	0.974591652	0.942105263
45	1114	60	50	1054	0.946140036	0.954710145	0.950405771
46	550	58	21	492	0.894545455	0.959064327	0.925682032
47	421	13	42	408	0.96912114	0.906666667	0.936854191
48	688	42	15	646	0.938953488	0.97730711	0.957746479
87	663	43	106	620	0.935143288	0.85399449	0.892728582
88	639	80	17	559	0.874804382	0.970486111	0.920164609
89	673	55	52	618	0.918276374	0.92238806	0.920327625
90	466	9	34	457	0.980686695	0.930753564	0.955067921
91	1036	36	81	1000	0.965250965	0.92506938	0.944733113
92	269	20	13	249	0.925650558	0.950381679	0.937853107
93	504	36	21	468	0.928571429	0.957055215	0.942598187
94	149	12	10	137	0.919463087	0.931972789	0.925675676
95	541	35	17	506	0.935304991	0.96749522	0.95112782
96	572	60	20	512	0.895104895	0.962406015	0.927536232
97	719	55	32	664	0.923504868	0.954022989	0.938515901
98	309	13	16	296	0.957928803	0.948717949	0.953301127
99	385	17	26	368	0.955844156	0.934010152	0.944801027
100	663	27	32	636	0.959276018	0.952095808	0.955672427
101	395	12	81	383	0.969620253	0.825431034	0.891734575
102	524	15	72	509	0.971374046	0.876075731	0.921266968
103	916	38	32	878	0.958515284	0.964835165	0.961664841
104	298	6	109	292	0.979865772	0.728179551	0.835479256
105	435	17	109	418	0.96091954	0.79316888	0.869022869
106	143	2	36	141	0.986013986	0.796610169	0.88125
107	772	89	23	683	0.884715026	0.967422096	0.924221922
					0.938425935	**0.926660914**	**0.931250897**

Table 2: Experimental results for stem cell images of group 1 by proposed method. For this group we obtained. in average. 93.84% of precision. 92.67% of recall and 93.12% of F-measure.

Image	Automatic Counting	FP	FN	TP	Precision	Recall	F-measure
64	272	29	35	243	0.893382353	0.874100719	0.883636364
65	273	13	66	260	0.952380952	0.797546012	0.868113523
66	407	26	40	381	0.936117936	0.904988124	0.920289855
67	184	5	42	179	0.972826087	0.809954751	0.883950617
68	231	10	50	221	0.956709957	0.815498155	0.880478088
069a	331	5	53	326	0.98489426	0.860158311	0.918309859
069b	308	11	34	297	0.964285714	0.897280967	0.929577465
70	232	13	40	219	0.943965517	0.845559846	0.892057026
71	255	5	23	250	0.980392157	0.915750916	0.946969697
72	1884	95	253	1789	0.949575372	0.876101861	0.911360163
073a	557	25	58	532	0.955116697	0.901694915	0.927637315
073b	685	34	64	651	0.950364964	0.91048951	0.93
74	809	54	53	755	0.933250927	0.934405941	0.933828077
75	1093	65	126	1028	0.94053065	0.890814558	0.914997775
76	778	33	71	745	0.957583548	0.912990196	0.934755332
77	1514	126	94	1388	0.91677675	0.9365722	0.926568758
78	1217	95	107	1122	0.921939195	0.912937347	0.91741619
79	1121	59	70	1062	0.947368421	0.938162544	0.942743009
80	1052	76	40	976	0.927756654	0.960629921	0.943907157
81	1329	92	58	1237	0.930775019	0.955212355	0.942835366
82	1421	119	67	1302	0.916256158	0.951059167	0.933333333
83	1848	88	79	1760	0.952380952	0.957041871	0.954705723
84	640	36	39	604	0.94375	0.939346812	0.941543258
85	511	25	35	486	0.951076321	0.932821497	0.941860465
86	767	76	36	691	0.900912647	0.950481431	0.925033467
					0.943214768	**0.903263997**	**0.921836315**

Table 3: Experimental results for stem cell images of group 2 by proposed method. For this group we obtained. in average. 94.32% of precision. 90.33% of recall and 92.18% of F-measure.

Image	ε	Automatic Counting	FP	FN	TP	Precision	Recall	F-measure
Figure 10a	16	399	4	1	395	0.989974937	0.997474747	0.993710692
Figure 10b	8	321	9	24	312	0.971962617	0.928571429	0.949771689
Figure 10c	16	44	3	0	41	0.931818182	1	0.964705882
Figure 10e	32	46	6	0	40	0.869565217	1	0.930232558
						0.940830238	**0.981511544**	**0.959605205**

Table 4: Experimental results for additional images by proposed method. For this images we obtained. in average. 94.08% of precision. 98.15% of recall and 95.96% of F-measure.